Bleton *et al. BMC Medical Imaging* (2016) 16:22
DOI 10.1186/s12880-016-0125-0

BMC Medical Imaging

RESEARCH ARTICLE Open Access

Cognitive tasks and cerebral blood flow through anterior cerebral arteries: a study via functional transcranial Doppler ultrasound recordings

Héloïse Bleton[1], Subashan Perera[2] and Ervin Sejdić[1*]

Abstract

Background: Functional transcanial Doppler ultrasound (fTCD) is a convenient approach to examine cerebral blood flow velocity (CBFV) in major cerebral arteries.

Methods: In this study, the anterior cerebral artery (ACA) was insonated on both sides, that is, right ACA (R-ACA) and left ACA (L-ACA). The envelope signals (the maximum velocity) and the raw signals were analyzed during cognitive processes, i.e. word-generation tasks, geometric tasks and resting state periods separating each task. Data which were collected from 20 healthy participants were used to investigate the changes and the hemispheric functioning while performing cognitive tasks. Signal characteristics were analyzed in time domain, frequency domain and time-frequency domain.

Results: Significant results have been obtained through the use of both classic/modern methods (i.e. envelope/raw, time and frequency/information-theoretic and time-frequency domains). The frequency features extracted from the raw signals highlighted sex effects on cerebral blood flow which revealed distinct brain response during each process and during resting periods. In the time-frequency analysis, the distribution of wavelet energies on the envelope signals moved around the low frequencies during mental processes and did not experience any lateralization during cognitive tasks.

Conclusions: Even if no lateralization effects were noticed during resting-state, verbal and geometric tasks, understanding CBFV in ACA during cognitive tasks could complement information extracted from cerebral blood flow in middle cerebral arteries during similar cognitive tasks (i.e. sex effects).

Keywords: Anterior cerebral arteries, Cerebral blood flow, Functional transcanial Doppler ultrasound, Signal processing

Background

Distribution patterns of cerebral blood flow can be described by neuroimaging techniques such as functional magnetic resonance imaging, single photon emission computed tomography, positron emission tomography or the xenon-clearance technique. All these methods have a high spatial resolution [1–4]. Despite their advantages, these methods restrict patient movements and usually have a low temporal resolution. The hemodynamic features of major cerebral arteries and their rapid variations in normal and pathological conditions can be characterized by functional transcanial Doppler ultrasound. Functional transcanial Doppler ultrasound (fTCD) is a non-invasive blood velocity measurement approach [5]. This technique uses the fact that cerebral perfusion is linked to neural activation which is translated into cerebral perfusion changes during cognitive tasks [6, 7]. It has a high temporal resolution due to continuous insonation of cerebral blood flow velocity. The velocity measurement is closely linked to cerebral blood flow in the event that the

*Correspondence: esejdic@ieee.org
[1] Department of Electrical and Computer Engineering, University of Pittsburgh, Pittsburgh, PA, USA
Full list of author information is available at the end of the article

diameter of cerebral arteries does not change during the insonation. Multiple studies showed that perfusion area and diameter of cerebral arteries do not change during mental processes [8–10]. Thus, blood flow velocity evolutions are due to modifications in cerebral metabolism because of cerebral activities.

fTCD has been studied during cognitive or physical tasks for both healthy participants and patients affected by neurological disorders (e.g., stroke, autism, epilepsy) [11–15]. Previous publications have examined the effects of visual perception [16, 17], auditory perception [18, 19], language processes [20, 21], spatial processes [22, 23], memory processes [24], other cognitive/mental tasks and other neurological disorders [13, 25, 26] on cerebral blood flow using fTCD. These publications pointed that the main advantages of a fTCD system include its price, easiness-to-use and its minimally stressful character [27].

fTCD is mainly used to target major cerebral arteries [28]. Usually, transducers are placed on the thinnest parts of head bone which are the acoustic windows of the skull allowing to monitor activities on cerebral arteries of the circle of Willis. The transtemporal window enables us to reach the middle (MCA), anterior (ACA) and posterior (PCA) cerebral arteries. The transforaminal window enables us to reach the basilar and the vertebral arteries; while the transorbital window reaches the ophthalmic and the internal arteries [29]. Arteries are identified by understanding the depth of insonation, the transducers position and the flow direction [30]. The most commonly insonated arteries are the ACA, the MCA and the PCA [31]. Each of these arteries supplies blood to different areas: the ACA supply to the medial regions, the MCA supply to the lateral regions and the PCA supply to the posterior basomedial regions. The MCA is most usually insonated in studies about cognitive processes [20, 32–34], as 80 % of blood to the brain is delivered by the MCA. The ACA could be also insonated during high cognitive functions such as arithmetic problems or receptive language [35–37]. As ACA are deeper than MCA [29], insonating ACA could provide complimentary information to signals acquired from MCA in order to gain further understanding of cerebral blood flow characteristics while performing mental activities [30, 38, 39].

Previous publications regarding cerebral blood flow velocities during mental stimuli on MCA highlighted the left and right hemispheric dominance introduced during the geometric task and the word-generation task respectively. However, the brain blood flow in ACA is closely linked to the activity in MCA [32, 33, 35]. In fact, lateralization in the ACA blood flow was predicted while performing cognitive processes (i.e. evolutions of cerebral blood flow velocity can be explained by the changes in the MCA during mental challenges). Moreover, handedness and sex appeared to have effects on brain response during activation periods. Distinct functioning hemispheric dominance may be foreseen according to sex and handedness [40].

Our hypothesis was that cognitive tasks affect the cerebral blood flow velocities in ACAs similarly to those changes observed in cerebral blood flow velocities in MCAs. To examine our hypothesis, we collected both raw signals and maximal velocity signals (usually called the spectral envelope signals [41]). A few fTCD studies only examined envelope signals and may lack information contained in raw signals [5, 31, 42]. Previous studies highlighted the significance of data embodied in raw signals during resting periods [43, 44]. Envelope signals are usually extracted from raw signals, which are a sum of signals corresponding to erythrocytes movement at different velocities. Raw results which are used to calculate envelope signals, may contain exhaustive information about the activation stimuli and resting-state periods.

Our major contributions include the understanding of signal patterns in various domains (time, frequency, and time-frequency) for raw and maximum velocity signals. Features from the classical analysis were examined (i.e. time and frequency approaches). We also used modern analysis characteristics from information-theoretic and time-frequency domains which have not been examined in previous studies about brain response during mental tasks [45]. Additionally, the current study complements the study of the ACA resting-state characteristics [43] and follows outcomes from MCA results during resting periods and activation stimuli (word-generation and geometric rotation tasks) [45]. These two previous papers employed the same methodology. The repercussions of sex and handedness on CBFV were also examined.

Methods

Subjects

Twenty able-bodied participants have taken part in the experiment (Males/Females = 9/11, 22.1 $\pm$ 1.86 years old; 171 $\pm$ 10.1 cm; 68.9 $\pm$ 27.3 kg). Table 1 summarizes participant demographic details. No participant had a history of heart murmurs, strokes, concussions, migraines or other brain-related injuries or neurological diseases. At first, the subjects were asked to sign the consent form approved by the University of Pittsburgh Institutional Review Board.

Table 1 Demographic information

Distribution	Male	Female	All
Age (years old)	22.3 $\pm$ 1.64	22.0±2.00	22.1±1.86
Height (cm)	180±7.26	163±5.39	171±10.1
Weight (kg)	91.6±29.3	52.6±5.89	68.9±27.3

The entire study was approved by the University of Pittsburgh Institutional Review Board.

The handedness of each participant was tested using the Edinburgh Handedness Inventory test [46]. This technique is one of the most widely used method for measuring both the direction and the degree of handedness [47, 48]. Subjects had to choose their hand preferences based on a list of activities. They could assign 1 or 2 for each activity (1 for a weak preference or 2 for a strict preference between right or left hand). The result was scored based on the formula:

$$Score = \frac{\sum X_i(R) - \sum X_i(L)}{\sum X_i(R) + \sum X_i(L)} \quad (1)$$

where $X_i(R)$ or $X_i(L)$ can take values of 0, 1 or 2 according to the domination of right/left domination. Positive score leads to right-handedness whereas negative score leads to left-handedness. This study was restricted to the analysis of handedness direction. In fact, a majority of previous publications about fTCD and brain cognitive response focused on the effects of handedness direction [35, 49, 50]. 16 subjects were right-handed (mean score of 64), 3 subjects were left-handed (mean score of -63) and one was ambidextrous. Table 2 summarizes the Edinburgh Handedness test results.

Procedure

ACA cerebral blood flow was assessed thanks to a SONARA TCD System (Carefusion, San Diego, CA, USA). Two 2 MHz transducers were placed on the left side and the right side of the skull on transtemporal windows to acquire bilateral cerebral blood flow measurements. The temporal windows are found above the zygomatic arch [38]. Transducers were fixed with a headset (5 cm in front of the ears) and were positioned to reach ACA. Additionally, the end-tidal carbon dioxide $ETCO_2$ (BCI Capnocheck Sleep Capnograph, Smiths Medical, Waukesha, Wisconsin, USA) was monitored along with respiration rate, electrocardiogram, head movement and skin conductance via a multisystem physiological data monitoring system (Nexus-X, Mindmedia, Netherlands). The $ETCO_2$ levels may have repercussions on cerebal blood flow in the ACA.

The participants were asked to complete two 15-minute cognitive parts interspersed by a 5-minute break. However, we did not collect data during these five minutes. Each 15-minute part comprises 5 mental rotation tasks, 5 word generation tasks and 5 resting conditions between each cognitive task. Each of these lasted for 45 seconds. The order of cognitive tasks was randomly assigned, but it was counterbalanced. Figures 1 and 2 illustrate the fTCD setup.

Table 2 Handedness information

Distribution	Right-Handed	Left-Handed	Ambidextrous
Sex	8 males, 8 females	1 male, 2 females	1 female
Average score	64	-63	0

After the acquisition of R-ACA and L-ACA cerebral blood flow data in the form of audio file, information are extracted from audio files sampled at 44100 Hz. Raw data were downsampled to 8820 Hz to speed up data processing.

Resting-state

During 5-minutes breaks and during the resting-state, participants were requested to remain awake, maintain a thought-free mental state and keep quiet.

Geometric rotation task

During the 45-seconds mental rotation tasks, pairs of images were randomly selected from a database constructed from 3-D cubes [51]. Pairs were displayed for 9 seconds each. Participants were asked to rotate shapes to find which ones are identical or mirror symmetrical.

Word generation task

Participants generated words silently based on letters randomly chosen and displayed at the beginning of each period. Subjects were cautioned not to vocalize any words in order to avoid any brain activations related to speech regions [52].

Feature extraction

Three common parameters in statistics were considered: standard deviation, skewness, kurtosis of the signal amplitude [53]. Statistical parameters from the envelope and the raw signals were extracted. Standard deviation of a signal estimates the spread of a distribution [53, 54]. The skewness of the amplitude distribution quantifies the asymmetry of the distribution [53, 55]. The kurtosis of a distribution evaluates the behavior of the distribution close to the boundaries [53]. These statistical features characterize signals from the right side and from the left side of ACA.

The cross-correlation coefficient at the zero lag between the L-ACA signal and the R-ACA signal was used to demonstrate whether L-ACA signal and R-ACA signal are related:

$$CC_{X_{R-ACA}/Y_{L-ACA}} = \frac{1}{N}\sum_{i=1}^{N}(x_i y_i) \quad (2)$$

where the signal $X_{R-ACA} = \{x_i\}$ and $Y_{L-ACA} = \{y_i\}$, $i = 1, \cdots, N$ are extracted from the right and the left side of the ACA.

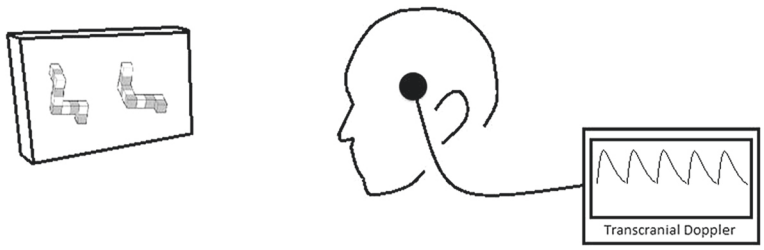

Fig. 1 Setup for the fTCD study

Information-theoretic feature

Information-theoretic features were also taken into consideration. The Lempel-Ziv complexity (LZC) and the entropy rate were extracted. These measures provide information about the complexity and the regularity of signals.

The amount of new patterns formation through finite time sequences is determined by the Lempel-Ziv complexity [56]. In fact, it estimates the predictability and the randomness of the signal [57, 58]. The Lempel-Ziv measure is often used in applications of analysis of biomedical signals [56, 59]. First, the signal amplitude is converted into a finite binary series. It is divided into 100 finite spaces defined thanks to 99 thresholds, T_h, $1 \leq h \leq 99$, $h \in \mathbb{Z}^+$. The threshold is usually chosen as the median of the signal [60]. Secondly, the quantized signal $X_1^n = \{x_1, x_2, \cdots, x_n\}$ is divided into blocks. Each block is series of successive data of length L. All block can be defined as the following formula [61]:

$$B = X_j^l = \{x_j, x_{j+1}, \cdots, x_l\}, 1 \leq j \leq l \leq n, j, l \in Z^+ \quad (3)$$

where the length L of the block is defined by $j - l + 1$. For each L, every block is tested from left to right. A counter c is defined and it increases by one unit if a block has not already appeared in previous j and l. Finally, the LZC is given as the following formula:

$$LZC = \frac{c(log_{100}c + 1)}{n} \quad (4)$$

where c denotes the final value of the counter at the end of the signal analysis and n represents the total of quantized levels in the signal.

The entropy rate ρ quantifies the regularity in a distribution [62]. First, the signal needs to be normalized to zero mean and unit variance (subtracting μ_X and dividing by σ_X) and quantized into 10 equal levels. The quantized signal $X = \{x_1, x_2, \cdots, x_n\}$ is decomposed and grouped into blocks of length L, $10 \leq L \leq 30$, which are finite series of consecutive points in the quantized signal such as $\Omega_L = \{\omega_1, \omega_2, \cdots, \omega_{n-L+1}\}$ [63].

$$\omega_i = 10^{L-1}x_{i+L-1} + 10^{L-2}x_{i+L-2} + \cdots + 10^0 x_i \quad (5)$$

where L is the length of successive series and ω_i is classified between 0 and $10^L - 1$. The Shannon entropy $S(L)$ of ω_L given the quantized signal Ω_L, where X takes discrete values ω_j with probability p_j is defined as [64]:

$$S(L) = \sum_{j=0}^{10^{L-1}} p_j ln p_j \quad (6)$$

where p_j is the approximated sample joint probability of the pattern j in Ω_L with the understanding that $\sum_{j=1}^{n-L+1} p_j = 1$ with $0 \leq p_j \leq 1\, i = 1, \cdots, n - L + 1$. The normalized entropy rate is computed as the following formula [65, 66]:

$$N(L) = \frac{S(L) - S(L-1) + S(1)pe(L)}{S(1)} \quad (7)$$

where $pe(L)$ is the percentage of the integers in the L-dimensional phase space that appeared only once and

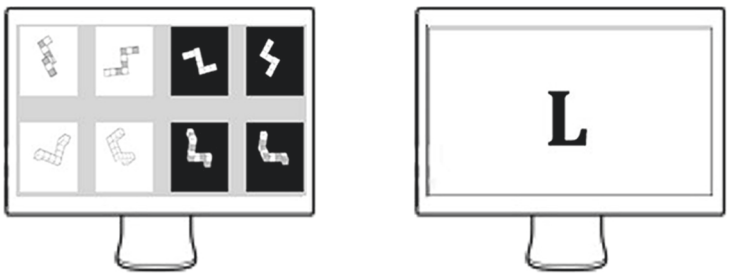

Fig. 2 A sample of the on-screen geometric and word-generation stimuli

Table 3 Time features from raw (denoted by the subscript r) and envelope (denoted by the subscript e) CBFV signals (* denotes multiplication by 10^{-3})

	Standard deviation		Skewness		Kurtosis		Cross-correlation
	R-ACA	L-ACA	R-ACA	L-ACA	R-ACA	L-ACA	
Rr	0.12 ± 0.05	0.12 ± 0.05	(-2.62 ± 0.15)*	(-0.59 ± 4.77)*	4.10 ± 2.06	4.43 ± 3.58	(5.67 ± 9.13)*
Wr	0.12 ± 0.05	0.12 ± 0.05	(-0.55 ± 9.02)*	0.89 ± 10.2)*	3.57 ± 0.90	4.26 ± 2.60	(6.96 ± 9.11)*
Gr	0.12 ± 0.04	0.12 ± 0.05	(-1.11 ± 9.38)*	(-1.26 ± 4.69)*	3.74 ± 0.95	4.42 ± 2.87	(6.50 ± 8.59)*
Re	15.9 ± 4.76	15.1 ± 5.98	1.17 ± 0.93	1.07 ± 0.58	5.95 ± 6.51	5.17 ± 2.52	0.89 ± 0.06
We	16.0 ± 4.72	15.2 ± 5.93	1.20 ± 0.90	1.13 ± 0.67	5.94 ± 6.16	5.50 ± 3.22	0.89 ± 0.06
Ge	15.9 ± 4.95	14.5 ± 5.87	1.03 ± 0.46	1.11 ± 0.63	4.74 ± 1.80	5.41 ± 2.79	0.90 ± 0.05

where $S(1)pe(L)$ is added due to the limited number of samples and the underestimation of $S(L) - S(L-1)$ for larger L. Given that the first term decreases while the second term increases with L, the goal of this method is looking for the minimum of the previous function. This minimum is an index of complexity. Finally, the regularity index ρ of the signal is defined by the following relation [66]:

$$\rho = 1 - min(N(L)) \tag{8}$$

where ρ is ranged from 0 which is equivalent to a maximal randomness to 1 which corresponds to a minimal regularity.

The cross-entropy rate quantifies the coupling of the entropy rate between two stochastic processes. It predicts data in a signal from previous and current information in another signal. Instead of making one signal normalized, both X and Y were processed (normalized, quantized and computed according to the previous method), yielding Ω_L^X and Ω_L^Y. Finally, the cross-entropy rate$\Omega_L^{X|Y}$ which represents the information rate available in one of the samples of the quantized signal x when a pattern of $L-1$ samples of the quantized signal y is established was constructed as [65]:

$$\omega_i^{X|Y} = 10^{L-1}x_{i+L-1} + 10^{L-2}y_{i+L-2} + \cdots + 10^0 y_i \tag{9}$$

The normalized cross-entropy NC of $X|Y$ is figured out as:

$$NC_{X|Y}(L) = \frac{S_{X|Y}(L) - S_Y(L-1) + S_X(1)pe_{X|Y}(L)}{S_X(1)} \tag{10}$$

where $S_X(L)$, $S_Y(L)$ and $S_{X|Y}$ represent the Shannon entropies of ω_L^X, ω_L^Y and $\omega_L^{X|Y}$. $pe_{X|Y}(L)$ is the rate of data in $\omega_L^{X|Y}$ that appeared only once and $S_X(1)pe_{X|Y}(L)$ is added due to the limited number of samples and the underestimation of $S_{X|Y}(L) - S_Y(L-1)$ for larger L. As the previous method, the goal is looking for the minimum of the previous function. The index of synchronization was used as the cross-entropy rate characteristic:

$$\Lambda_{X|Y} = 1 - min(NC_{X|Y}(L), NC_{Y|X}(L)) \tag{11}$$

where $\Lambda_{X|Y}$ is between 0 which denotes that X and Y are independent processes and 1 which proves a synchronization of X and Y.

Frequency analysis

Spectral changes of the recorded signals were examined through the peak frequency, the centroid frequency, the bandwidth of the spectrum [67, 68]. The peak frequency is associated with the maximal spectral power:

$$f_p = arg_f max\{|F_X(f)|^2\} \tag{12}$$

where $F_X(f)$ is the Fourier transform of the signal X and f_{max} in this study was 8820 Hz. The spectral centroid is defined as the center of gravity of the spectrum [69]:

$$f_c = \frac{\int_0^{f_{max}} f|F_X(f)|^2 \, \mathrm{d}f}{\int_0^{f_{max}} |F_X(f)|^2 \, \mathrm{d}f} \tag{13}$$

The bandwidth of the spectrum which represents the difference between the higher and lower frequencies of the spectrum measures the spreadness of the frequency components:

$$B = \sqrt{\frac{\int_0^{f_{max}} (f - \widehat{f})^2 |F_X(f)|^2 \, , \mathrm{d}f}{\int_0^{f_{max}} |F_X(f)|^2 \, , \mathrm{d}f}} \tag{14}$$

The bandwidth represents the squared differences between the spectral centroid and the spectral components.

Table 4 Significant time features from raw (denoted by the subscript r) and envelope (denoted by the subscript e) CBFV signals where $p < 0.05$

Signal	ACA	Feature	Group	Group 1	Group 2
e	R-ACA	Skewness	R	M: 1.81 ± 1.09	F: 0.91 ± 0.73
e	R-ACA	Skewness	W	M: 1.50 ± 1.13	F: 0.95 ± 0.50
e	L-ACA	Skewness	G	M: 1.40 ± 0.63	F: 0.87 ± 0.62
e	R-ACA	Kurtosis	R	M: 9.21 ± 8.01	F: 4.80 ± 3.08

Table 5 Information-theoretic features from raw (denoted by the subscript r) and envelope (denoted by the subscript e) CBFV signals

	LZC		Entropy rate		Index synchronization
	R-ACA	L-ACA	R-ACA	L-ACA	
Rr	0.69 ± 0.03	0.68 ± 0.04	0.30 ± 0.14	0.35 ± 0.19	0.33 ± 0.17
Wr	0.69 ± 0.02	0.68 ± 0.03	0.28 ± 0.13	0.34 ± 0.18	0.32 ± 0.16
Gr	0.69 ± 0.02	0.68 ± 0.04	0.30 ± 0.14	0.37 ± 0.19	0.34 ± 0.17
Re	0.67 ± 0.04	0.67 ± 0.03	0.06 ± 0.07	0.04 ± 0.06	0.14 ± 0.08
We	0.67 ± 0.04	0.68 ± 0.03	0.06 ± 0.07	0.04 ± 0.06	0.14 ± 0.08
Ge	0.68 ± 0.03	0.67 ± 0.03	0.05 ± 0.05	0.04 ± 0.06	0.17 ± 0.10

Time-frequency analysis

A 10-level discrete wavelet decomposition of the signal using the discrete Meyer wavelet was calculated. The resulting decomposition is given by $W = [\, a_{10}\, d_{10}\, d_9 \cdots d_1]$ where a_{10} is the approximation coefficients and d_k represents detail coefficients at the k^{th}-level. The signal is observed at various frequency bands thanks to this new distribution [70]. Then, the relative energy from the approximation coefficients is defined as [71]:

$$\Xi_a = \frac{\|a_{10}\|^2}{\|a_{10}\|^2 + \sum_{k=1}^{10} \|d_k\|^2}(\%) \tag{15}$$

$$\Xi_{d_k} = \frac{\|d_k\|^2}{\|a_{10}\|^2 + \sum_{k=1}^{10} \|d_k\|^2}(\%) \tag{16}$$

where $\|.\|$ is the Euclidian norm. The relative energy which is defined by the ratio of the energy at the kth level divided by the total energy was calculated based on the wavelet transform. It denotes the distribution of energies at different frequency bands.

A wavelet entropy measures the amount of order of the signal and gives information about the distribution [71, 72]:

$$\Omega = -\Xi_{a_{10}} log_2 \Xi_{a_{10}} - \sum_{k=1}^{10} \Xi_{d_k} log_2 \Xi_{d_k} \tag{17}$$

where $\Xi_{a_{10}}$ is the relative energy. A value of Ω close to 0 demonstrates a concentration of wavelet energies in a fine band of levels even though a higher value of Ω proves an extensive band of levels (a random process).

Statistical test

To make comparisons across sex, within tasks, types of measurements and sides in a unified manner, we fitted a series of linear mixed models with each feature as the dependent variable; sex (male/female), task (geometric/verbal/resting), measurement type (raw/envelope), side (left/right) and their full multi-way interaction as independent factors; and a subject random effect to account for multiple measurements from each participants and the resulting non-independence of observations. Next, combining both sex, to make comparisons between the levels of each of the task, measurement type and side factors within the combinations of other factors, we fit a similar mixed model but only with task, measurement type, side and their interaction as independent factors. In each case, appropriately constructed means contrasts were used to estimate the pairwise means differences of interest reported here, along with their statistical significance and 95 % confidence intervals. For cross-correlation and synchronization index features which are not side specific, we employed a largely similar strategy but omitted side from the list of independent factors. SAS version 9.3 (SAS Institute, Inc., Cary, North Carolina) was used for the mixed model analysis. MATLAB (MathWorks, Natick, MA, United States) was used for feature extraction.

Results

Firstly, the effect of the end-tidal carbon dioxide level which does not influence features (ACA diameter) is not taken into consideration [73, 74], as we did not observe any relations between signal features and end-tidal carbon dioxide levels. Furthermore, participants did not exhibit any excessive head movements. Secondly, feature values for the raw and the envelope signals are displayed in tables in the form of (*mean* ± *standarddeviation*) according to experimental conditions: the 45-seconds resting-state is indicated by a "R", the word-generating task is indicated by a "W" and the geometric task is indicated by a "G" in the

Table 6 Significant information-theoretic features from raw (denoted by the subscript r) and envelope (denoted by the subscript e) CBFV signals where $p < 0.05$

Signal	ACA	Feature	Group	Group 1	Group 2
e	R-ACA	LZC	R	M: 0.65 ± 0.04	F: 0.69 ± 0.04
e	L-ACA	LZC	R	M: 0.66 ± 0.03	F: 0.70 ± 0.04
e	R-ACA	LZC	W	M: 0.65 ± 0.04	F: 0.68 ± 0.03
e	L-ACA	LZC	W	M: 0.66 ± 0.04	F: 0.69 ± 0.04

Table 7 Frequency features from raw (denoted by the subscript r) and envelope (denoted by the subscript e) CBFV signals

	Spectral centroid		Peak frequency		Bandwidth	
	R-ACA	L-ACA	R-ACA	L-ACA	R-ACA	L-ACA
Rr	980 ± 193	939 ± 213	561 ± 308	564 ± 214	723 ± 116	564 ± 214
Wr	994 ± 184	950 ± 208	540 ± 239	584 ± 221	723 ± 116	696 ± 151
Gr	990 ± 192	939 ± 211	567 ± 269	527 ± 257	718 ± 120	690 ± 152
Re	13.3 ± 4.50	14.0 ± 4.30	0.36 ± 0.50	0.23 ± 0.46	13.5 ± 1.73	13.5 ± 1.43
We	13.5 ± 4.62	14.0 ± 4.30	0.38 ± 0.51	0.39 ± 0.55	13.5 ± 1.74	13.6 ± 1.47
Ge	13.5 ± 4.5	14.1 ± 4.36	0.45 ± 0.55	0.33 ± 0.51	13.5 ± 1.60	13.5 ± 1.37

tables. Using the calculated feature values, we examined the effects of lateralization, sex, handedness and tasks on the features. A, F, M, RH and LH denote "all participants", "female participants", "male participants", "right-handed participants" and "left-handed participants," respectively.

Time features

Table 3 presents time feature values for all participants in the raw and the envelope signals while Table 4 shows significant results in time domain concerning the handedness and sex effects in time domain.

No significant statistical difference was established for raw CBFV signals. On the opposite side, a few meaningful results were detected between sex on the envelope signals. Male subjects had higher skewness than female participants in R-ACA signals during resting-state ($p = 0.01$) and during verbal challenge ($p = 0.02$). A rise of skewness was noticed on the left ACA signals in the case of men during geometric task ($p = 0.02$). Additionally, larger kurtosis was observed for men on the R-ACA during the 45-seconds resting period ($p = 0.03$).

Information-theoretic features

A summary of information-theoretic feature values and statistical differences (handedness and sex effects) in information-theoretic approach are presented in Tables 5 and 6 for the raw and the envelope signals.

Multiple comparison test revealed significant results on LZC between sex on the envelope signals during resting periods and during word-generation challenges. Female had higher LZC in the R-ACA and the L-ACA signals during both periods ($p < 0.05$).

Frequency-domain features

Tables 7 and 8 present frequency feature values and significant results (handedness and sex effects) in the raw and the envelope signals.

Meaningful results were only noticed on sex in raw CBFV signals. The spectral centroid of raw R-ACA CBFV signals increased in the case of women during cognitive challenges and 45-seconds resting period ($p < 0.02$). Moreover, the bandwidth values of R-ACA was larger from female results during rest/verbal/geometric processes ($p < 0.05$).

Time-frequency features

Table 9, Fig. 3 and Fig. 4 present the wavelet entropy values and the feature values of wavelet energy decomposition for raw and the envelope signals. Table 10 shows significant results for both signals (handedness and sex effects).

The multiple comparison test revealed signal information in time-frequency domain. Sex had effects on R-ACA and L-ACA raw signals. The relative energy d_{10} of R-ACA outcomes increased in the case of women during resting state and during mental processes ($p < 0.02$), while decreasing in R-ACA and L-ACA d_7 in the case of women during rest periods and cognitive tasks ($p < 0.04$). For envelope results, cognitive challenges had some impact on R-ACA and L-ACA envelope signals in comparison with the baseline results, i.e. 45-seconds resting periods. A lower wavelet entropy was highlighted on both sides of ACA during cognitive processes ($p < 0.04$).

On the other hand, 94 % of energy were concentrated around the approximation band a_{10} for the envelope signals. Therefore, for these signals, we only considered the a_{10} level. Statistical differences in R-ACA and L-ACA a_{10} were noticed: the mental periods showed larger a_{10} than rest periods ($p < 0.02$).

Table 8 Significant frequency features from raw (denoted by the subscript r) and envelope (denoted by the subscript e) CBFV signals where $p < 0.05$

Signal	ACA	Feature	Group	Group 1	Group 2
r	R-ACA	Spectral Centroid	R	M: 855 ± 198	F: 1090 ± 225
r	R-ACA	Spectral Centroid	W	M: 913 ± 204	F: 1060 ± 181
r	R-ACA	Spectral Centroid	G	M: 896 ± 203	F: 1066 ± 192
r	R-ACA	Bandwidth	R	M: 641 ± 107	F: 734 ± 118
r	R-ACA	Bandwidth	W	M: 675 ± 137	F: 763 ± 139
r	R-ACA	Bandwidth	G	M: 665 ± 141	F: 760 ± 138

Table 9 Wavelet entropy values for raw and envelope CBFV signals

		RAW		ENVELOPE	
		R-ACA	L-ACA	R-ACA	L-ACA
Wavelet entropy	R	2.10 ± 0.23	2.12 ± 0.25	0.50 ± 0.19	0.47 ± 0.17
	W	2.07 ± 0.17	2.10 ± 0.22	0.39 ± 0.17	0.36 ± 0.16
	G	2.07 ± 0.19	2.12 ± 0.26	0.40 ± 0.18	0.35 ± 0.13

Comparison between raw and envelope signals

Results demonstrated differences between raw signals and envelope signals and showed low p-values except for results in Table 11.

Discussion

Raw and envelope signals were significantly different as demonstrated by the features describing their probability density functions. No effect of handedness was found on time domain features while the sex effects were exhibited on the R-ACA and L-ACA raw and envelope signals. Higher kurtosis proved that the CBFV variations are grouped around one value [75], while larger skewness highlighted higher signal assymetry [53]. R-ACA envelope signals from female participants seemed more dispersive and more symmetrical than from male subjects during the rest and verbal periods. Hence, the cerebral blood flow changed with a wider range in females than in males during resting-state and word-generation processes on the right side of ACA.

Time-domain outcomes did not reveal differences between signal characteristics during resting-state periods and during mental challenges. For example, the cross-correlation value was close to zero for raw signals implying low signal dependence in the time domain. Previous studies highlighted the dependence of signals between the two sides of MCA and the evolution of blood flow velocity during cognitive processes. Lateralization was introduced during the geometric task and the word-generation task. It was shown that there was a hemispheric lateralization due to an increase of the cerebral blood flow velocity during cognitive tasks [32, 33, 35]. The geometric task led to a dominance of R-MCA while the verbal task results in a dominance of L-MCA. Moreover, the cerebral blood flow in MCA is closely linked to the flow in ACA. Thus, an identical hemispheric dominance should be identified using results from ACA. Changes in the ACA blood flow and the possible lateralization observed in the flow can be explained by the changes in the MCA blood flow while performing cognitive processes. Nonetheless, time domain results from the current ACA study did not confirm cerebral lateralization during mental challenges.

Raw signals and envelope signals showed distinct cerebral blood flow characteristics which demonstrated the significance of extraction of envelope signals and preservation of raw signals from a statistical point of view. The envelope signals also had higher standard deviation and skewness than the raw signals. Raw signals centralized information around a value because of lower skewness and standard deviation. However, envelope signals exhibited higher cross-correlation values ($CC > 0.89$) than raw signals which proved that there was a low dependence on raw signals in the time domain.

When considering the information theoretic domain, sex effects were observed on randomness and complexity of the envelope signals. In fact, the Lempel-Ziv complexity exhibited differences between men and women. Right-sided and left-sided envelope signals from women were more complex than signals from men during resting-state period and word-generation processes. Rest periods and verbal tasks implied that the left and right ACA blood flow speed was distinguishable between men and women. Indeed, the envelope signals vary with higher fluctuations in the case of women.

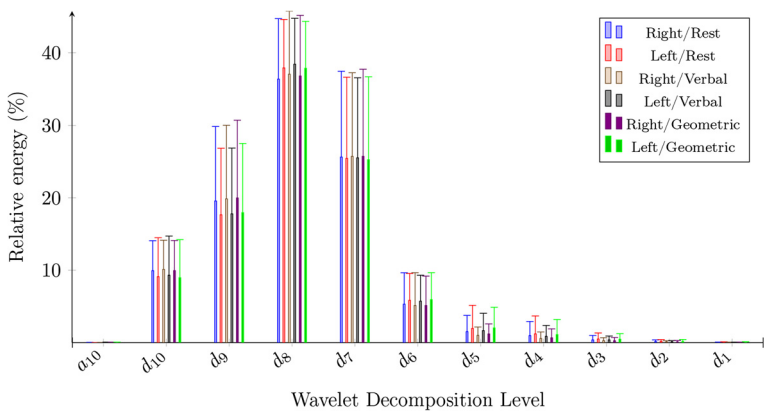

Fig. 3 The 10th level wavelet decomposition of raw signals

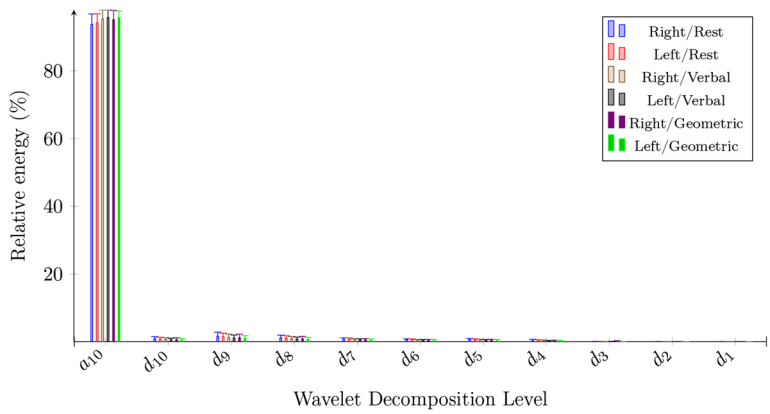

Fig. 4 The 10th level wavelet decomposition of envelope signals

In the frequency domain, raw signals exhibited higher frequency characteristics than envelope signals. As a matter of fact, envelope signals revealed a low-pass structure, while the raw signals presented a band-pass structure. When differentiating sex effects, spectral centroid frequencies and bandwidth of R-ACA raw signals from female participants had higher values than those from men during the geometric task. This finding implied an increase of right-sided blood flow above baseline was more pronounced for women than for men during geometric tasks. Sex differences during mental stimuli have been widely studied, particularly during spatial challenges. Previous publications underlined distinct hemispheric dominance seen in women and in men [40, 76, 77]. Women revealed activation of other right brain regions during geometric tasks [76]. It could be explained by two distinct strategies of task solving/the anatomical brain structure/sex hormones [78–81]. A rise of centroid frequency was also noticed during the resting-state and verbal tasks. It appeared that female subjects showed a higher right-sided CBFV baseline. These distinct baseline metabolisms may be caused by emotional brain responses (i.e. sex hormones) or by anatomical brain differences [79–82]. The frequency domain analysis did not indicate the existence of handedness-based difference.

From the time-frequency point of view, lower wavelet entropy values highlighted that right-sided and left-sided envelope signals were more ordered during cognitive periods than during 45-second resting-state periods. In addition, the rise of wavelet energy a_{10} proved that cognitive tasks led to modifications of CBFV signals comparing to resting state. Time-frequency outcomes did not expose major changes into brain functioning during mental tasks. We did not observe neither handedness nor sex effects on a_{10} values for R-ACA and L-ACA raw and envelope signals.

The uneven small number of subjects in each group may also be important limitation in the outcomes about the sex effects (i.e. 20 subjects) and handedness effects on brain response (i.e. 16 right-handed and 3 left-handed subjects). Therefore, the results obtained after analyzing comparisons between right and left-handed subjects and between male and female participants are not as pronounced. Given the low number of ambidextrous

Table 10 Significant time-frequency features from raw (denoted by the subscript r) and envelope (denoted by the subscript e) CBFV signals where $p < 0.05$

Signal	ACA	Feature	Group	Group 1	Group 2
r	R-ACA	$\Xi_{d_{10}}$	R	M: 6.92 ± 3.08	F: 11.4 ± 4.71
r	R-ACA	$\Xi_{d_{10}}$	W	M: 8.23 ± 4.05	F: 11.7 ± 3.25
r	R-ACA	$\Xi_{d_{10}}$	G	M: 7.90 ± 4.09	F: 11.7 ± 3.35
r	R-ACA	Ξ_{d_7}	R	M: 32.9 ± 12.0	F: 19.1 ± 8.02
r	L-ACA	Ξ_{d_7}	R	M: 30.3 ± 12.5	F: 21.2 ± 9.08
r	R-ACA	Ξ_{d_7}	W	M: 29.8 ± 12.2	F: 22.4 ± 9.73
r	L-ACA	Ξ_{d_7}	W	M: 29.7 ± 11.2	F: 22.1 ± 9.64
r	R-ACA	Ξ_{d_7}	G	M: 30.4 ± 12.7	F: 21.9 ± 9.97
r	L-ACA	Ξ_{d_7}	G	M: 29.5 ± 11.4	F: 21.8 ± 10.2

Table 11 Absence of statistical difference between raw and envelope CBFV signals where $p > 0.06$

Multiple	Rest periods		Verbal tasks		Geometric tasks	
	R-ACA	L-ACA	R-ACA	L-ACA	R-ACA	L-ACA
Kurtosis	A, F	A, M, F	F	A, M, F	A, M, F	A, M, F
LZC	F	A, M, F	F	A, M, F	A, M, F	A, M, F
Ξ_{d_5}	M, F	M	A, M, F	M	A, M, F	M
Ξ_{d_4}	A		A		A	
Ξ_{d_2}	M		M	M	M	
Ξ_{d_1}	A, M, F	A, M, F	A, M, F	A, M, F	A, M, F	M, F

participants (i.e. 1 ambidextrous subject), we examined the significant *p*-values between right and left-handed participants.

Conclusions

In this study, the evolution of the cerebral blood flow velocities in left and right ACA was investigated during three different tasks: a mental rotation task, a word generation task and resting periods between cognitive tasks. Characteristics of the raw signals and the envelope signals were analyzed in time, frequency, and time-frequency domains. Significant results have been obtained through the use of both classic/modern methods (i.e. envelope/raw, time and frequency/information-theoretic and time-frequency domains). The time and the information-theoretic results underlined modifications of shape distribution and randomness. The acquired data in the frequency domain presented a low-pass characteristic in the case of envelope signals while the raw signals presented band-pass characteristics. In the time-frequency analysis, the distribution of wavelet energies for the envelope signals was around the low frequencies during cognitive activities. Finally, differences were obtained for the raw and envelope signals based on sex effects. Distinct hemispheric functioning between men and women was highlighted during each process. A few significant statistical differences demonstrated the different brain response.

Competing interests

The authors declare that they have no competing interests.

Authors' contributions

ES conceived the experiment. HB collected and analyzed data. SP conducted the statistical analysis of the results. HB, SP and ES wrote the manuscript. All authors read and approved the final manuscript.

Acknowledgements

The work was supported by the Pittsburgh Older Americans Independence Center (NIA P30 AG024827).

Author details

[1]Department of Electrical and Computer Engineering, University of Pittsburgh, Pittsburgh, PA, USA. [2]Division of Geriatric Medicine, University of Pittsburgh, Pittsburgh, PA, USA.

Received: 3 December 2015 Accepted: 29 February 2016
Published online: 12 March 2016

References

1. Phelps ME. PET: a biological imaging technique. Neurochem Res. 1991;16(9):929–40.
2. Fiez JA. Neuroimaging studies of speech. An overview of techniques and methodological approaches. J Commun Disorders. 2001;34(6):445–54.
3. Khalil MM, Tremoleda JL, Bayomy TB, Gsell W. Molecular SPECT imaging: an overview. Int J Mol Imaging. 2011;2011(Article ID 796025):1–15.
4. Thomas DJ, Zilkha E, Redmond S, Du Boulay GH, Marshall J, Ross Russell RW, Symon L. An intravenous Xenon clearance technique for measuring cerebral blood flow. J Neurol Sci. 1979;40(1):53–63.
5. Aaslid A, Markwalder TM, Nornes H. Noninvasive transcranial Doppler ultrasound recording of flow velocity in basal cerebral arteries. J Neurosurg. 1982;57(6):769–74.
6. Deppe M, Ringelstein EB, Knecht S. The investigation of functional brain lateralization by transcranial Doppler sonography. Neuroimage. 2004;21(3):1124–46.
7. Fox PT, Raichle ME. Focal physiological uncoupling of cerebral blood flow and oxidative metabolism during somatosensory stimulation in human subjects. Proc Nat Acad Sci USA. 1986;83(4):1140–44.
8. Huber P, Handa J. Effect of contrast material, hypercapnia, hyperventilation, hypertonic glucose and papaverine on the diameter of the cerebral arteries. Angiographic determination in man. Invest Radiol. 1967;2(1):17–32.
9. Giller CA, Bowman G, Dyer H, Mootz L, Krippner W. Cerebral arterial diameters during changes in blood pressure and carbone dioxide during craniotomy. Neurosurgery. 1993;32(5):737–42.
10. Kontos HA. Validity of cerebral arterial blood flow calculations from velocity measurements. Stroke. 1989;20(1):1–3.
11. Saqqur M, Uchino K, Demchuk AM, Molina CA, Garami Z, Calleja S, Akhtar N, Orouk FO, Salam A, Shuaib A, Alexandrov AV. Site of arterial occlusion identified by transcranial Doppler predicts the response to intravenous thrombolysis for stroke. Stroke. 2007;38(3):948–54.
12. Burgin WS, Malkoff M, Felberg RA, Demchuk AM, Christou I, Grotta JC, Alexandrov AV. Transcranial Doppler ultrasound criteria for recanalization after thrombolysis for middle cerebral artery stroke. Stroke. 2000;31(5):1128–32.
13. Knake S, Haag A, Hamer HM, Dittmer C, Bien S, Oertel WH, Rosenow F. Language lateralization in patients with temporal lobe epilepsy: a comparison of functional transcranial Doppler sonography and the Wada test. NeuroImage. 2003;19(3):1228–32.
14. Juhász C, Scheidl E, Szirmai I. Reversible focal mri abnormalities due to status epilepticus. an eeg, single photon emission computed tomography, transcranial doppler follow-up study. Electroencephalogr Clin Neurophysiol. 1998;107(6):402–7.
15. Whitehouse A, Bishop D. Cerebral dominance for language function in adults with specific language impairment or autism. Brain. 2008;131(12):3193–200.
16. Aaslid R. The Doppler Principle Applied to Measurement of Blood Velocities in Cerebral Arteries. Vienna: Springer; 1986.
17. Conrad B, Klingelhöfer J. Dynamics of regional cerebral blood flow for various visual stimuli. Exp Brain Res. 1989;77(2):437–41.
18. Vollmer-Haase J, Finke K, Hartje W, Bulla-Hellwig M. Hemispheric dominance in the processing of J.S, Bach fugues: a transcranial Doppler sonography (TCD) study with musicians. Neuropsychologia. 1998;36(9):857–67.
19. Evers S, Dannert J, Rödding D, Rötter G, Ringelstein EB. The cerebral haemodynamics of music perception. A transcranial Doppler sonography study. Brain. 1999;122(1):75–85.
20. Markus HS, Boland M. "Cognitive Activity" monitored by non-invasive measurement of cerebral blood flow velocity and its application to the investigation of cerebral dominance. Cortex. 1992;28(4):575–81.
21. Stroobant N, Buijs D, Vingerhoets G. Variation in brain lateralization during various language tasks: a functional transcranial Doppler study. Behav Brain Res. 2009;199(2):190–6.
22. Kelley RE, Chang JY, Suzuki S, Levin BE, Reyes-Iglesias Y. Selective increase in the right hemisphere transcranial Doppler velocity during a spatial task. Cortex. 1993;29(1):45–52.
23. Schnittger C, Johannes S, Münte TF. Transcranial Doppler assessment of cerebral blood flow velocity during visual spatial selective attention humans. Neurosci Lett. 1996;214(1):41–4.
24. Cupini LM, Matteis M, Troisi E, Sabbadini M, Bernardi G, Caltagirone C, Silvestrini M. Bilateral simultaneous transcranial Doppler monitoring of flow velocity changes during visuospatial and verbal working memory tasks. Brain. 1996;119(4):1249–53.
25. Silvestrini M, Caltagirone C, Cupini LM, Matteis M, Troisi E, Bernardi G. Activation of healthy hemisphere in poststroke recovery. A transcranial Doppler study. Stroke. 1993;24(11):1673–7.
26. Trabold F, Meyer S, Blanot PG, Carli GA, Orliaguet PA. The prognostic value of transcranial Doppler studies in children with moderate and severe head injury. Intensive Care Med. 2004;30(1):108–12.
27. Schmidt P, Krings T, Willmes K, Roessler F, Reul J, Thron A. Determination of cognitive hemispheric lateralization by "functional" Transcranial Doppler cross-validated by functional MRI. Stroke. 1999;30(5):939–45.
28. Reid JM, Spencer MP. Ultrasonic Doppler technique for imaging blood vessels. Science. 1972;176(4040):1235–6.

29. White H, Venkatesh B. Applications of transcranial Doppler in the ICU: a review. Intensive Care Med. 2006;32(7):981–4.
30. Alexandrov AV, Sloan MA, Wong LKS, Douville C, Razumovsky AY, Koroshetz M, Kaps WJ, Tegeler CH. Practice standards for transcranial Doppler ultrasound: part i– test performance. J Neuroimaging. 2007;17(1): 11–8.
31. Duschek S, Schandry R. Functional transcranial Doppler sonography as a tool in psychophysiological research. Psychophysiology. 2003;40(3): 436–54.
32. Droste DW, Harders AG, Rastogi E. A transcranial Doppler study of blood flow velocity in the middle cerebral arteries performed at rest and during mental activities. Stroke. 1989;20(8):1005–11.
33. Hartje W, Ringelstein EB, Kistinger B, Fabianek D, Willmes K. Transcranial Doppler ultrasonic assessment of middle cerebral artery blood flow velocity changes during verbal and visuospatial cognitive tasks. Neuropsychologia. 1994;32(12):1443–52.
34. Matteis M, Bivona U, Catani S, Pasqualetti P, Formisano R, Vernieri F, Troisi E. Functional transcranial Doppler assessment of cerebral blood flow velocities changes during attention tasks. Eur J Neurol. 2009;16(1):81–7.
35. Vingerhoets G, Stroobant N. Lateralization of cerebral blood flow velocity changes during cognitive task: a simultaneous bilateral transcranial Doppler study. Stroke. 1999;30(10):2152–158.
36. Kelley RE, Chang JY, Scheinman NJ, Levin BE, Duncan RC, Lee SC. Transcranial Doppler assessment of cerebral flow velocity during cognitive tasks. Stroke. 1992;23(1):9–14.
37. Vingerhoets G, Stroobant N. Reliability and validity of day-to-day blood flow velocity reactivity in a single subject: an fTCD study. Ultrasound Med Biol. 2002;2(28):197–202.
38. DeWitt LD, Wechsler LR. Transcranial Doppler. Stroke. 1988;19(7):915–21.
39. Lennihan L, Petty GW, Fink ME, Solomon RA, Mohr JP. Transcranial Doppler detection of anterior cerebral artery vasospasm. J Neurol Neurosurg Psychiat. 1993;56(8):906–9.
40. Gur R, Gur R, Obrist W, Hungerbuhler J, Younkin D, Rosen A, Skolnick B, Reivich M. Sex and handedness differences in cerebral blood flow during rest and cognitive activity. Science. 1982;217(4560):659–61.
41. Deppe M, Knecht S, Henningsen H, Ringelstein EB. Average: a Windows ®program for automated analysis of event related cerebral blood flow. J Neurosci Methods. 1997;75(2):147–54.
42. Wechsler LR, Ropper AH, Kistler JP. Transcranial Doppler in cerebrovascular disease. Stroke. 1986;17(5):905–12.
43. Huang H, Sejdić E. Assessment of resting-state blood flow through anterior cerebral arteries using transcranial Doppler recordings. Ultrasound Med Biol. 2013;39(12):2285–94.
44. Sejdić E, Kalika D, Czarnek N. An analysis of resting-state functional transcranial Doppler recordings from middle cerebral arteries. PloS ONE. 2013;8(2):55405.
45. Li M, Huang H, Boninger M, Sejdić E. An analysis of cerebral blood flow from middle cerebral arteries during cognitive tasks via functional transcranial Doppler recordings. Neurosci Res. 2014;84:19–26.
46. Oldfield RC. The assessment and analysis of handedness: The edinburgh inventory. Neuropsychologia. 1971;9(1):97–113.
47. Dragovic M. Categorization and validation of handedness using latent class analysis. Acta Neuropsychiatrica. 2004;16(4):212–8.
48. Dassonville P, Zhu X, Ugurbil K, Kim S, Ashe J. Functional activation in motor cortex reflects the direction and the degree of handedness. Proc Nat Acad Sci USA. 1997;94(25):14015–8.
49. Stroobant N, Vingerhoets G. Transcranial Doppler ultrasonography monitoring of cerebral hemodynamics during performance of cognitive tasks: a review. Neuropsychol Rev. 2000;10(4):213–31.
50. Hartje W, Ringelstein EB, Kistinger B, Fabianek D, Willmes K. Transcranial Doppler ultrasonic assessment of middle cerebral artery blood flow velocity changes during verbal and visuospatial cognitive tasks. Neuropsychologia. 1994;32(12):1443–52.
51. Peters M, Battista C. Applications of mental rotation figures of the Shepard and Metzler type and description of a mental rotation stimulus library. Brain Cogn. 2008;66(3):260–4.
52. Silvestrini M, Cupini L, Matteis M, Troisi E, Caltagirone C. Bilateral simultaneous assessment of cerebral flow velocity during mental activity. J Cereb Blood Flow Metab. 1994;14(4):643–8.
53. Papoulis A. Probability, Random Variables, and Stochastic Processes. New York: WCB/McGraw-Hill; 1991.
54. Zoubir AM, Boashash B. The bootstrap and its application in signal processing. IEEE Signal Process Mag. 1998;15(1):56–76.
55. Allen J, Coan J, Nazarian M. Issues and assumptions on the road from raw signals to metrics of frontal EEG assymetry in emotion. Biol Psychol. 2004;67(1–2):183–218.
56. Aboy M, Hornero R, Abàsolo D, Àlvarez D. Interpretation of the Lempel-Ziv Complexity measure in the context of biomedical signal Analysis. IEEE Trans Biomed Eng. 2006;53(11):2282–8.
57. Szczepański J, Amigò J, Wajnryb E, Sanchez-Vives. Characterizing spike trains with Lempel-Ziv Complexity. Neurocomputing. 2004;58–60:79–84.
58. Ahmed S, Shahjahan M, Murase K. A Lempel-Ziv Complexity-based neural network pruning algorithm. Int J Neural Syst. 2011;21(5):427–41.
59. Nagarajan R. Quantifying physiological data with Lempel-Ziv quantifying physiological data with Lempel-Ziv Complexity–Certain issues. IEEE Trans Biomed Eng. 2002;49(11):1371–3.
60. Hu J, Gao J, Principe J. Analysis of biomedical signals by the Lempel-Ziv Complexity: the effect of finite data size. IEEE Trans Biomed Eng. 2006;53(12):2606–9.
61. Lempel A, Ziv J. On the complexity of finite sequences. IEEE Trans Inform Theory. 1976;22(1):75–81.
62. Amigò J, Szczepański J, Wajnryb E, Sanchez-Vives M. Estimating the entropy rate of spike trains via Lempel-Ziv Complexity. Neural Comput. 2004;16(4):717–36.
63. Porta A, Guzzetti S, Montano N, Furlan R, Pagani M, Somers V. Entropy, entropy rate, and pattern classification as tools to typify complexity in short heart period variability series. IEEE Trans Inform Theory. 2011;48(11): 1282–91.
64. Bezerianos A, Tong S, Thakor N. Time-dependent entropy estimation of EEG rhythm changes following brain ischemia. Ann Biomed Eng. 2003;31(2):221–32.
65. Porta A, Baselli G, Lombardi F, Montano N, Malliani A, Cerutti S. Conditional entropy approach for the evaluation of the coupling strength. Biol Cybernet. 1999;81(2):119–29.
66. Porta A, Baselli G, Liberati D, Montano N, Cogliati C, Gnecchi-Ruscone T, Malliani A, Cerutti S. Measuring regularity by means of a corrected conditional entropy in sympathetic outflow. Biol Cybernet. 1998;78(1): 71–8.
67. Sejdić E, Djurović I, Jiang J. Time-frequency feature representation using energy concentration: an overview of recent advances. Digital Signal Process. 2009;19(1):153–83.
68. Lee J, Sejdić E, Steele CM, Chau T. Effects of liquid stimuli on dual-axis swallowing accelerometer signals in a healthy population. Biomed Eng Online. 2010;9(1):7.
69. Tzanetakis G, Cook P. Musical genre classification of audio signals. IEEE Trans Speech Audio Process. 2002;10(5):293–302.
70. Hilton M. Wavelet and wavelet packet compression of electrocardiograms. IEEE Trans Biomed Eng. 1997;44(5):394–402.
71. Rosso OA, Blanco S, Yordanova J, Kolev V, Figliola A, Schürmann M, Basar E. Wavelet entropy: a new tool for analysis of short duration brain electrical signals. J Neurosci Methods. 2001;105(1):65–75.
72. Robertson D, Camps O, Mayer J, Gish W. Wavelet and electromagnetic power system transients. IEEE Trans Power Delivery. 1996;11(2):1050–8.
73. Jordan J, Shannon JR, Diedrich A, Black B, Costa F, Robertson D, Biaggioni I. Interaction of carbon dioxide and sympathetic nervous system activity in the regulation of cerebral perfusion in humans. Hypertension. 2000;36(3):383–8.
74. Serrador J, Picot P, Rutt B, Shoemaker J, Bondar R. MRI measures of middle cerebral artery diameter in conscious humans during simulated orthostasis. Stroke. 2000;31(7):1672–8.
75. DeCarlo L. On the meaning and use of kurtosis. Psychol Methods. 1997;2(3):292–307.
76. Weiss E, Siedentopf C, Hofer A, Deisenhammer E, Hoptman M, Kremser C, Golaszewski S, Felber S, Fleischhacker W, Delazer M. Sex differences in brain activation pattern during a visuospatial cognitive task: a functional magnetic resonance imaging study in healthy volunteers. Neurosci Lett. 2003;344(3):169–72.
77. Gur R, Alsop D, Glahn D, Petty R, Swanson C, Maldjian J, Turetsky B, Detre J, Gee J, Gur R. An fMRI study of sex differences in regional activation to a verbal and a spatial task. Brain Lang. 2000;74(2):157–70.
78. Thomsen T, Hugdahl K, Ersland L, Barndon R, Lundervold A, Smievoll A, Roscher B, Sundberg H. Functional magnetic resonance imaging (fMRI)

study of sex differences in a mental rotation task. Med Sci Monitor. 2000;6(6):1186–96.
79. Marinoni M, Ginanneschi A, Inzitari D, Mugnai S, Amaducci L. Sex-related differences in human cerebral hemodynamics. Acta Neurologica Scandinavica. 1998;97(5):324–7.
80. Good C, Johnsrude I, Johnsrude J, Henson R, Friston K, Frackowiak S. Cerebral asymmetry and the effects of sex and handedness on brain structure: a voxel-based morphometric analysis od 465 normal adult human brains. NeuroImage. 2001;14(3):685–700.
81. Cosgrove K, Mazure C, Staley J. Evolving knowledge of sex differences in brain structure, function and chemistry. Biol Psychiat. 2007;62(8):847–55.
82. Gur R, Gur R, Mozley P, Mozley L, Resnick S, Karp J, Alavi A, Arnold S. Sex differences in regional cerebral glucose metabolism during a resting-state. Science. 1995;267(5197):528–31.